Planetary and Space Science 61 (2012) 108–113

Contents lists available at ScienceDirect

Planetary and Space Science

journal homepage: www.elsevier.com/locate/pss

A despeckle filter for the Cassini synthetic aperture radar images of Titan's surface

Emmanuel Bratsolis [a,*], Georgios Bampasidis [a,b], Anezina Solomonidou [b,c], Athena Coustenis [b]

[a] Faculty of Physics, University of Athens, Athens GR-15784, Greece
[b] LESIA, Observatoire de Paris - Meudon, 92195 Meudon Cedex, France
[c] Faculty of Geology and Geoenvironment, University of Athens, Athens GR-15784, Greece

ARTICLE INFO

Article history:
Received 24 December 2010
Received in revised form
30 March 2011
Accepted 7 April 2011
Available online 18 May 2011

Keywords:
Titan
Lakes
Radar imaging
Filtering
Segmentation

ABSTRACT

Cassini synthetic aperture radar (SAR) images of Titan, the largest satellite of Saturn, reveal surface features with shapes ranging from quasi-circular to more complex ones, interpreted as liquid hydrocarbon deposits assembled in the form of lakes or seas. One of the major problems hampering the derivation of meaningful texture information from SAR imagery is the speckle noise. It overlays real structures and causes gray value variations even in homogeneous parts of the image. We propose a filtering technique which can be applied to obtain restored SAR images. Our technique is based on probabilistic methods and regards an image as a random element drawn from a prespecified set of possible images. The despeckle filter can be used as an intermediate step for the extraction of regions of interest, corresponding to structured units in a given area or distinct objects of interest, such as lake-like features on Titan. This tool can therefore be used, among other, to study seasonal surficial changes of Titan's polar regions. In this study we also present a segmentation technique that allows us to separate the lakes from the local background.

1. Introduction

Cassini–Huygens, the extremely successful NASA/ESA joint mission to the Saturnian system, has already accomplished six years of extended investigation. Titan being one of the most intriguing objects in the Solar system, hosting an Earth-like environment, is one of the main targets of this mission. Titan's landscape has been observed by multiple flybys that examine the surface expressions through Cassini's infrared and radar instrumentation.

Cassini's RADAR instrument operates in the Ku-band (13.78 GHz, $\lambda = 2.17$ cm), at both high and low resolution, viewing Titan's surface in four modes: imaging, altimetry, scatterometry and radiometry (Elachi et al., 2004).

The SAR mode is used at altitudes lower than 4000 km, resulting in spatial resolution ranging from about 350 m to more than 1 km. Images are acquired either left or right of nadir using 1–5 looks while a swath, 120–450 km in width, is created from five antenna beams. SAR coverage is dependent on spacecraft range and orbital geometry (Elachi et al., 2004) and radar backscatter variations in SAR images can be interpreted in terms of variations of surface geometry (incidence angle, azimuth angle, and the polarization vector), near-surface roughness, or near-surface dielectric properties.

The images obtained using SAR revealed that Titan hosts a very complex surface formed with features such as lakes, mountains, fluvial river networks, possible volcanic-like features and dunes (Jaumann et al., 2008; Lopes et al., 2010 and references therein) which resemble Earth-like geomorphological structures (Coustenis and Hirtzig, 2009). However, both the material and the environmental conditions shaping their respective surfaces are considerably different. Despite these differences, the exogenic mechanisms forming the surficial expressions may be similar. Indeed, one dominating terrestrial surface-affecting procedure is the water cycle while on Titan an active methane cycle is at play (Atreya et al., 2006). The impact of the endogenic processes in the surface construction on Titan is still under investigation through geophysical interior models (e.g. Tobie et al., 2005). Radar images provided evidence of drainage and branching channel networks with subdivided channels (Perron et al., 2006; Soderblom et al., 2007; Lorenz et al., 2008; Burr et al., 2009), as well as distinct fluvial erosional patterns (Jaumann et al., 2008) that indicate dynamic and evolved surface processes. Additionally, SAR imagery observed lake-like features in several swaths (Stofan et al., 2007; Turtle et al., 2009; Hayes et al., 2010; Wye et al., 2010).

Other features, identified by radar, are the potentially volcanic in origin structures (Elachi et al., 2005; Lopes et al., 2007a; Soderblom et al., 2009; Nelson et al., 2009; Wall et al., 2009), the impact craters

* Corresponding author. Tel.: +30 2105813069.
E-mail address: ebrats@phys.uoa.gr (E. Bratsolis).

0032-0633/$ - see front matter © 2011 Published by Elsevier Ltd.
doi:10.1016/j.pss.2011.04.003

(Wood et al., 2010), the mountain chains (e.g. Radebaugh et al., 2007) and the linear dunes (Elachi et al., 2006; Radebaugh et al., 2008).

2. Lacustine features of Titan's surface

The thermodynamical conditions dominating Titan as well as its chemical profile allow the hydrocarbon liquid phase to exist on its surface (Kouvaris and Flasar, 1991; Thompson et al., 1992; Atreya et al., 2006). Indeed, the temperature of its icy surface has been measured in situ (10.34°S, 192.34°W) (Tomasko et al., 2005) by Huygens at 93.7 K (Fulchignoni et al., 2005), while the Cassini composite infrared spectrometer (CIRS) found by remote observations an average temperature of 92 K between 2004 and 2008 (Jennings et al., 2009).

Cassini RADAR instrumentation confirmed the presence of lake-like features on the surface of Titan. Several models have suggested organic precipitation on Titan (Toon et al., 1988; Lorenz, 1993; Graves et al., 2008) either violently through torrential storms (Hueso and Sanchez-Lavega, 2006) or smoothly through drizzle at the lower atmosphere (Tokano et al., 2006) and rainfalls originated from occasional short-lived clouds (Griffith et al., 2000, 2005; Lorenz et al., 2005), such phenomena have not been recorded yet.

The first recording of organic liquid pools was accomplished during the T16 flyby at the northern polar locations, where more than 75 lake candidate features were identified (Sotin, 2007; Stofan et al., 2007). In 2008, the Cassini/RADAR swaths counted in both north and south polar regions, above 50°N and 50°S, respectively, more than 655 lake-like features (Hayes et al., 2008). SAR imaging shows lake-like features separated into three classes: dark lakes, granular lakes, and bright lakes (Hayes et al., 2008). Dark lakes are interpreted as liquid filled, while bright lakes are interpreted as empty basins and granular lakes are inferred as transitional between dark and bright lake features. From a geomorphological aspect the lakes on Titan span over the range of observed morphologies on Earth (Stofan et al., 2007; Mitri et al., 2007; Hayes et al., 2008). They are rimmed features, from circular to irregular and some with distinct edges, steep margins and smooth surfaces (Stofan et al., 2007) and they show very low microwave backscatter. Some of them are surrounded by a drainage network of dark channels, which may supply them with liquid (Stofan et al., 2007), while some are not.

It is suggested that this liquid is a methane/ethane mixture, with smaller concentrations of nitrogen and higher order hydrocarbons/nitriles (Lunine et al., 1983; Mitri et al., 2007; Brown et al., 2008; Raulin, 2008).

The lakes' radiometric brightnesses which appear to be warmer than the surrounding region (Janssen et al., 2009) are consistent with the high emissivity expected for a smooth surface with the real part of the low dielectric constant between 1.7 and 1.9 of liquid ethane–methane solutions (Lopes et al., 2007b) with most possible value the 1.9. However, the imaginary part is still under investigation (Notarnicola et al., 2009).

This study provides a qualitative method of recognition of lake-like features from Cassini SAR images. The intended goal is to label regions in an image into three classes (dark lakes, granular lakes and the local background). First, a filtering technique is applied to obtain the restored image. Then, a method of supervised segmentation is used. The segmentation method based on the minimum Euclidean distance is used here.

3. Filtering

Strip mapping SAR consists of a large antenna which is synthesized from many small antennas and remains fixed with respect to the radar platform, so that the large antenna illuminates a strip of the ground. This technique is used to improve the azimuthal resolution. As the platform moves, a sequence of closely spaced pulses is emitted and the returned waveforms are recorded. An image is computed after the coherent sum of reflected monochromatic microwaves. The image is distorted by a strong granulation, called speckle. Speckle noise exists in all types of coherent imaging systems and its presence reduces the resolution of the image and the detectability of the target. Speckle noise is not only signal dependent but is also spatially correlated and reduces the effectiveness of image reduction. The Cassini RADAR measures the normalized backscatter cross-section (σ_0) of Titan's surface (Ulaby et al., 1982). The SAR textures are generally affected by multiplicative speckle noise. In order to reduce the speckle noise, the multilook technique, based on incoherently averaging the independent neighboring pixels, is used to estimate the characteristics of the same ground area.

The statistical characteristics of multilook data depart considerably from those of single-look data. Multilook data tend to mix some physical and statistical properties of the terrain. The terrain appears more homogeneous and the multilook averaging will tend to be close to the Gaussian statistics (Chitroub et al., 2002).

Speckle noise overlays real structures and causes gray value variations even in homogeneous parts of the image and also makes automatic segmentation of such images difficult. We propose here a filtering technique that can be applied to obtain the SAR restored images. After filtering the structured parts of the image can be much better separated. The total sum preserving regularization (TSPR) filter, is based on a membrane model Markov random field approximation optimized by a synchronous local iterative method (Bratsolis and Sigelle, 2003). The final form of despeckling gives a sum-preserving regularization for the pixel values of the image.

Image formation is the process of computing (or refining) an image both from raw sensor data that is related to that image and from prior information about that image. Information about the image is contained in the raw sensor data, and the task of image formation is to extract this information so as to compute the image.

Image space is the set $\mathcal{F}$ of model images that represent the true, underlying physical distributions that are measured by the sensors.

Working in a probabilistic imaging problem, an a priori knowledge about an image is most naturally incorporated through the use of a prior probability distribution (or prior) $P(f)$ on the image space. Our objective here is to reconstruct the original (or true) image from its degraded version.

A random field is an appropriate model for image values. Random variables characterized by conditional priors that account for local interactions are often used as natural and convenient priors in imaging problems. These priors are placed directly on the image space. However, the fundamental probability distribution on the field is the joint probability distribution $P(f)$, and this is difficult or impossible to specify directly. One needs to verify that the chosen specification of conditional distributions is sufficient and consistent in the sense that a unique joint probability distribution corresponds to this set of conditional probability distributions.

Assume that an image is formed on a finite rectangular lattice when the sensors of this lattice select one scene from $\mathcal{F}$. Let us note the finite lattice of sites as $S=\{s\}_{s=1\ldots N}$ with $S\subset Z^2$. Each site $s\in S$ has a set of neighbors r noted $\mathcal{N}_s$. If $s=(i,j)$ four-connectivity is assumed in the following : $\mathcal{N}_s=\{(i-1,j);(i+1,j);(i,j-1);(i,j+1)\}$.

A random process $\{f_s|s\in S\}$ with f_s random variables following the joint probability function $P(f)$ is a "random field". In the special case where $P(f_s|\{f_r\neq s\})=P(f_s|\{f_r\}_{r\in\mathcal{N}_s})$ the random field is

called a "Markov random field" (MRF). By the Hammersley–Clifford theorem MRFs and Gibbs random fields on a finite lattice are equivalent under the positivity condition (Besag, 1974).

Let g be the degraded observed image and f the restored image. The general problem is now to estimate f from a set of input data g.

The Bayes theorem allows us to obtain the a posteriori probability for the field f given the data g:

$$P(f|g)=\frac{P(g|f)P(f)}{P(g)} \tag{1}$$

where $P(f)$ is the a priori probability for the field f, $P(g|f)$ is the conditional probability for the data g given f and $P(g)$ is the probability of g, which is independent of f.

Considering a multilook image, we assume for the conditional probability $P(g|f)$ a Gaussian distribution (Chitroub et al., 2002) and we have

$$P(g|f)=\frac{\exp-\left[\sum_s \frac{(f_s-g_s)^2}{2\sigma^2}\right]}{C_1} \tag{2}$$

where σ is the standard deviation of the Gaussian distribution and C_1 a normalization constant.

The probability $P(f)$ is given by

$$P(f)=\frac{\exp-\left[\beta\sum_{(r,s)}(f_s-f_r)^2\right]}{C_2} \tag{3}$$

where β is a smoothness factor, C_2 a normalization constant, and the sum runs on all pairs of neighboring sites. From (1) we obtain

$$P(f|g)=\frac{1}{Z}\exp-U(f) \tag{4}$$

where Z, also called the a posteriori partition function, is a normalization constant and $U(f)$ is the total a posteriori potential function, which is written as

$$U(f)=\sum_s \frac{(f_s-g_s)^2}{2\sigma^2}+\beta\sum_{(r,s)}(f_s-f_r)^2 \tag{5}$$

The related local conditional potential functions are given by

$$V_s(f)=\frac{(f_s-g_s)^2}{2\sigma^2}+\beta\sum_{r\in\mathcal{N}_s}(f_s-f_r)^2 \tag{6}$$

The a posteriori usual maximum (MAP) estimate is assigned to the value f which maximizes (4), i.e. which minimizes the a posteriori energy $U(f)$ (Bratsolis and Sigelle, 2003). We accept as a fast method of optimization a synchronous minimization of the local potential energies which we named synchronous local iterative method.

Our final TSPR filter is an iterative filter which uses the equation given by

$$f^{(n+1)}=\lambda g+(1-\lambda)\mathcal{R}*f^{(n)} \quad \forall n\geq 1 \tag{7}$$

where $*$ is the 2-D convolution operation. Thus, at each step the current pixel value will depend in a regularizing manner on its neighboring ones, according to the magnitude of parameter λ. It is also obvious that positivity is preserved when $0\leq\lambda\leq 1$. $\mathcal{R}$ is a normalized matrix given by

$$\mathcal{R}=\begin{bmatrix}0 & 0.25 & 0\\ 0.25 & 0 & 0.25\\ 0 & 0.25 & 0\end{bmatrix}$$

According to the notation of our method, it is evident that $\sigma_0=g_s$ and $\langle\sigma_0\rangle=\langle g_s\rangle=\langle f_s\rangle$. The TSPR method preserves the mean values of local homogeneous regions and decreases the standard deviation up to six times (Bratsolis and Sigelle, 2003).

4. The segmentation method

The purpose of segmentation is to divide the image into specific regions that correspond to structural units in the scene or distinguish objects of interest. These regions are characterized by spatially connected, non-overlapping sets of pixels sharing common properties.

In general, image segmentation is a classification problem. A classification problem can be formalized as a pair $(\mathcal{O},\mathcal{C})$, where $\mathcal{O}$ denotes a set of objects and $\mathcal{C}$ a collection of disjoint subsets $\mathcal{C}_1,\ldots,\mathcal{C}_l$ that partitions $\mathcal{O}$. The problem is to determine the subset $\mathcal{C}_j\subset\mathcal{C}$ to which a given object $o\in\mathcal{O}$ belongs. The supervised method of minimum Euclidean distance uses the mean values (or vectors) of each member and calculates the Euclidean distance from each classified object to the nearest class segmenting the image into different regions of interest or different labels (Richards, 1999). In our case we choose three regions of interest: dark lakes (black label), granular lakes (dark gray label) and local background (light gray label). The TSPR filter can be used as an intermediate step before the extraction of the regions of interest.

As Euclidean distance here, we define the distance

$$d_e=\sqrt{(f_s-\mu_i)^2} \tag{8}$$

where μ_i with $i=1,\ldots,3$ presents the mean values ($\langle\sigma_0\rangle$) corresponding to three sampled regions of interest. The algorithm is applied for every site s and for every value f_s of the restored (filtered) image. The value μ_i which minimize the distance d_e gives the characteristic label (black, dark gray or light gray) to the segmented image of Fig. 4, where μ_1 corresponds to -20.27 db, μ_2 to -18.64 db and μ_3 to -13.78 db.

We begin our analysis with the Cassini SAR image (PIA08630, NASA/JPL) acquired during the T16 flyby on July 22, 2006, at high latitudes near the north pole. This image is centered near 80°N, 92°W. Our image has dimensions 750×3100 in pixel size and the pixel scale is set to 175.558 m per pixel ($\sim 256^{\circ}$), but the actual SAR resolution is around 350 m per pixel and the image has been subjected to some interpolation. Cassini SAR images across this region contain numerous very dark splotches with sharp-edged boundaries, which may be filled with hydrocarbon liquid.

After using the despeckling filter TSPR we apply the segmentation method. Figs. 1 and 2 illustrate the initial image derived form the Cassini SAR while Fig. 3 is the filtering result of the previous image. The despeckling TSPR filter is used to smooth out the multiplicative

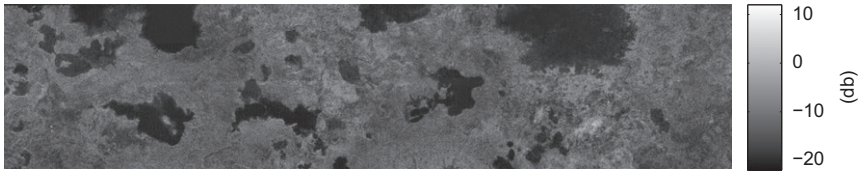

Fig. 1. Initial image of lakes (PIA08630, NASA/JPL) after subtraction of negative σ_0.

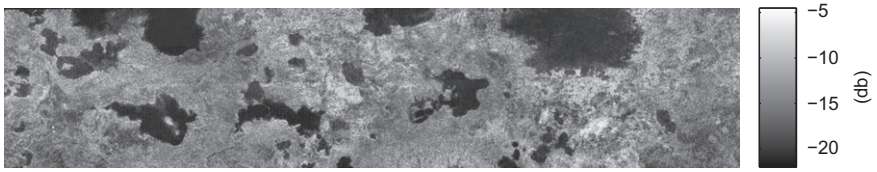

Fig. 2. Initial image of lakes (PIA08630, NASA/JPL) after subtraction of negative σ_0 and subtraction of values greater than $\langle\sigma_0\rangle+3\ std(\sigma_0)$.

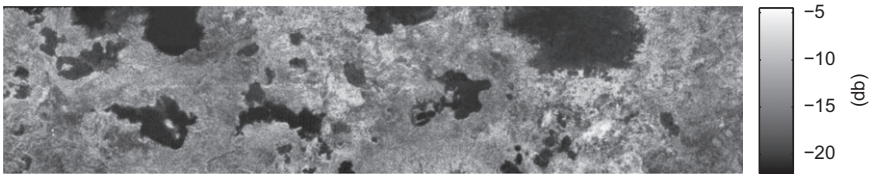

Fig. 3. Filtered image.

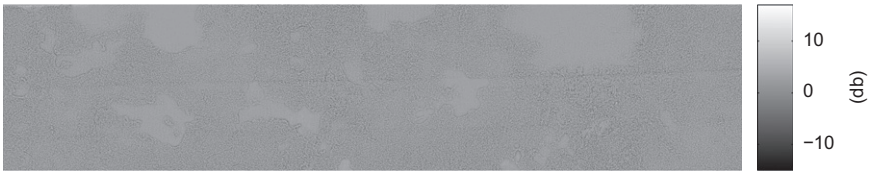

Fig. 4. Image ratio between the initial (Fig. 2) and the despeckled (Fig. 3) image.

Table 1
Characteristics of the sampled regions of interest.

Regions of interest	Before filtering $\langle\sigma_0\rangle \pm\ std(\sigma_0)$ (db)	After filtering $\langle\sigma_0\rangle \pm\ std(\sigma_0)$ (db)
Region 1 (black)	-20.27 ± 0.44	-20.26 ± 0.13
Region 2 (dark gray)	-18.64 ± 2.03	-18.53 ± 0.69
Region 3 (light gray)	-13.78 ± 3.57	-13.19 ± 1.32

noise of SAR images without missing important textural details from the regions of interest. Consequently, Fig. 3 seems smoother than Fig. 2. Fig. 4 depicts the ratio between the initial and the despeckle image. In this figure the lakes' interior is presented smoother than the surrounding area. This can be explained as the dark lakes are not really speckled regions. From the initial data (and σ_0 in non-dimensional values) the samples of the region 2 (granular lake) and the region 3 (local background) we take a value for the ratio $std(\sigma_0)/\langle\sigma_0\rangle$ equal to 0.4 and for the region 1 (dark lakes) equal to 0.05 which means that the region 1 is flatter than we were waiting.

The characteristics of the sampled regions of interest are listed in Table 1.

We can see the segmentation results in Fig. 5, where the black area corresponds to the dark lakes, the dark gray to the granular lakes and the light gray to the local background.

5. Discussion

Titan is indeed an active planetary body and both endogenic and exogenic processes have most possibly left their marks on the surface. Hence, one should focus on the surface geomorphology in order to identify any local tectonic field and estimate the importance as well as influence of each forming mechanism.

The TSPR filter, in combination with the minimum Euclidean distance method of supervised segmentation, can be used to extract regions of interest on the surface of Titan, such as lakes or seas using Cassini SAR images. Such despeckle filter can be applied in studying other surface features on Titan like the drainage networks, the equatorial dunes and the impact craters, where different textures appear.

Our approach allows to isolate each distinct surface feature from its surroundings and to study their distribution through out the surface. Then, in combination with radiative transfer modeling using Cassini visual and infrared mapping spectrometer (VIMS) data, we can infer about the relation between surface composition and morphotectonic structures. When we determine in a more accurate way the shapes of several surface structures, we will be able to study their global distribution and perform effectively classifications.

Since the Cassini mission extended its operational duration, new swaths, overlapping the liquid areas, have shown that the lakes have been evolving during the past years. Recent studies, focused on lake Ontario, the largest lake of the southern hemisphere, showed a significant recession of its shoreline (Turtle et al., 2009; Hayes et al., 2010; Wall et al., 2010) and support the hypothesis that these liquid deposits are not stable structures but evolve with time by expanding in winter and shrinking in the summer (Sotin, 2007). Applying the segmentation method on the same area at various periods of time, we can identify possible enhancements or reductions of the liquid coverage of the region. In particular, the temporal variation of the dark spots can provide information on the evolution of the lake system and consequently help us to better understand the methane cycle on Titan and therefore the mechanisms linked with the lake surface features, their origin and fate, through a global temporal and spatial coverage.

The passage from qualitative to quantitative results, requires to apply the aforementioned method in the same regions of interest with the same observational characteristics at different time periods in order to measure the surface each time.

Using this temporal dataset will help us evaluate the volume variation through time and estimate the hydrocarbon loss rate,

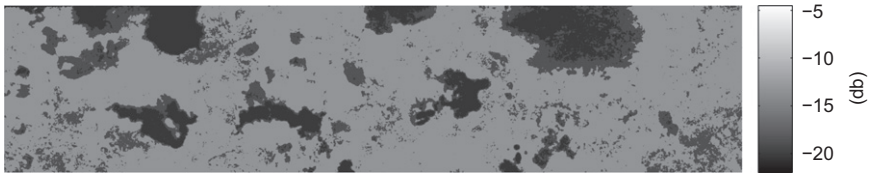

Fig. 5. Segmented image after filtering.

a critical parameter for the global methane cycle (Atreya et al., 2006).

Cassini evolves in the Saturnian system since 2004 and will continue returning data until at least 2017 in the extended mission. Although Cassini SAR recordings have unveiled new characteristics of Titan's surface, more advanced instrumentation with higher resolution is necessary to give a full picture of this complex environment.

A new long-term mission to Titan which will perform efficient in situ experiments in order to study widely the nature and the dynamics of its environment would be required.

Several proposals have been studied to this end. Recently, the 2008 study of a flagship mission, Titan Saturn System Mission (TSSM), focused on Titan and Enceladus exploration (Reh et al., 2008; Coustenis et al., 2009). TSSM consists of an orbiter, a lake lander and a balloon (montgolfière) and aims to a complete investigation scrutinizing thoroughly the whole satellite from the exosphere to its interior. The montgolfière would contain advanced instrumentation such as the Titan radar sounder ($>$ 150 MHz), which could perform a detailed surface investigation. In addition to topography, the radars on both the orbiter and the montgolfière would provide extended information regarding the lakes coverage. The proposed filtering and segmentation method in this paper would be a helpful tool in enhancing the return of the analysis of all SAR data acquired on Titan and other objects as well as in the exploitation of future missions to Titan.

Acknowledgments

The authors would like to gratefully acknowledge the assistance of Dr. Alexander Hayes in providing us with raw SAR Cassini data and with a thorough and constructive review of the manuscript and subsequent fruitful discussions. We are also grateful to another anonymous referee for helpful comments and suggestions.

A. Solomonidou is supported by the "HRACLEITOS II" project, co-financed by Greece and the European Union.

References

Atreya, S.K., Adams, E.Y., Niemann, H.B., Demick-Montelara, J.E., Owen, T.C., Fulchignoni, M., Ferri, F., Wilson, E.H., 2006. Titan's methane cycle. Planetary and Space Science 54, 1177–1187.

Besag, J., 1974. Spatial interaction and the statistical analysis of lattice systems (with discussion). Journal of the Royal Statistical Society Series B 36, 192–236.

Bratsolis, E., Sigelle, M., 2003. Fast SAR image restoration, segmentation and detection of high-reflectance regions. IEEE Transactions on Geoscience and Remote Sensing 41, 2890–2899.

Brown, R.H., Soderblom, L.A., Soderblom, J.M., Clark, R.N., Jaumann, R., Barnes, J.W., Sotin, C., Buratti, B., Baines, K.H., Nicholson, P.D., 2008. The identification of liquid ethane in Titan's Ontario Lacus. Nature 454, 607–610.

Burr, D.M., Jacobsen, R.E., Roth, D.L., Phillipis, C.B., Mitchell, K.L., Viola, D., 2009. Fluvial network analysis on Titan: evidence for subsurface structures and west-to-east wind flow, southwestern Xanadu. Geophysical Research Letters 36, L22203.

Chitroub, S., Houacine, A., Sansal, B., 2002. Statistical characterization and modeling of SAR images. Signal Processing 82, 69–92.

Coustenis, A., Hirtzig, M., 2009. Cassini–Huygens results on Titan's surface. Research in Astronomy and Astrophysics 9, 249–268.

Coustenis, A., Atreya, S., Balint, T., Brown, R., Dougherty, M., Ferri, F., Fulchignoni, M., Gautier, D., Gowen, R., Griffith, C., Gurvits, L., Jaumann, R., Langevin, Y., Leese, M., Lunine, J., McKay, C., Moussas, X., Muller-Wodarg, I., Neubauer, F., Owen, T., Raulin, F., Sittler, E., Sohl, F., Sotin, C., Tobie, G., Tokano, T., Turtle, E., Wahlund, J.E., Waite, J., Baines, K., Blamont, J., Coates, A., Dandouras, I., Krimigis, T., Lellouch, E., Lorenz, R., Morse, A., Porco, C., Hirtzig, M., Saur, J., Spilker, T., Zarnecki, J., Choi, E., Achilleos, N., Amils, R., Annan, P., Atkinson, D., Benilan, Y., Bertucci, C., Bezard, B., Bjoraker, G., Blanc, M., Boireau, L., Bouman, J., Cabane, M., Capria, M., Chassefière, E., Coll, P., Combes, M., Cooper, J., Coradini, A., Crary, F., Cravens, T., Daglis, I., de Angelis, E., de Bergh, C., de Pater, I., Dunford, C., Durry, G., Dutuit, O., Fairbrother, D., Flasar, F., Fortes, A., Frampton, R., Fujimoto, Galand, M., Grasset, O., Grott, M., Haltigin, T., Herique, A., Hersant, F., Hussmann, H., Ip, W., Johnson, R., Kallio, E., Kempf, S., Knapmeyer, M., Kofman, W., Koop, R., Kostiuk, T., Krupp, N., Kuppers, M., Lammer, H., Lara, L.M., Lavvas, P., Le Moulic, S., Lebonnois, S., Ledvina, S., Li, J., Livengood, T., Lopes, R., Lopez-Moreno, J.J., Luz, D., Mahaffy, P., Mall, U., Martinez-Frias, J., Marty, B., McCord, T., MenorSalvan, C., Milillo, A., Mitchell, D., Modolo, R., Mousis, O., Nakamura, M., Neish, C., Nixon, C., Nna Mvondo, D., Orton, G., Paetzold, M., Pitman, J., Pogrebenko, S., Pollard, W., Prieto-Ballesteros, O., Rannou, P., Reh, K., Richter, L., Robb, F., Rodrigo, R., Rodriguez, S., Romani, P., Ruiz Bermejo, M., Sarris, E., Schenk, P., Schmitt, B., Schmitz, N., Schulze-Makuch, D., Schwingenschuh, K., Selig, A., Sicardy, B., Soderblom, L., Spilker, L., Stam, D., Steele, A., Stephan, K., Strobel, D., Szego, K., Szopa, C., Thissen, R., Tomasko, M., Toublanc, D., Vali, H., Vardavas, I., Vuitton, V., West, R., Yelle, R., Young, E., 2009. TandEM: Titan and Enceladus mission. Experimental Astronomy 23, 893–946.

Elachi, C., Allison, M.D., Borgarelli, L., Encrenaz, P., Im, E., Janssen, M.A., Johnson, W.T.K., Kirk, R.L., Lorenz, R.D., Lunine, J.I., Muhleman, D.O., Ostro, S.J., Picardi, G., Posa, F., Rapley, C.G., Roth, L.E., Seu, R., Soderblom, L.A., Vetrella, S., Wall, S.D., Wood, C.A., Zebker, H.A., 2004. Radar: the Cassini Titan Radar Mapper. Space Science Reviews 115, 71–110.

Elachi, C., Wall, S., Allison, M., Anderson, Y., Boehmer, R., Callahan, P., Encrenaz, P., Flamini, E., Franceschetti, G., Gim, Y., Hamilton, G., Hensley, S., Janssen, M., Johnson, W., Kelleher, K., Kirk, R., Lopes, R., Lorenz, R., Lunine, J., Muhleman, D., Ostro, S., Paganelli, F., Picardi, G., Posa, F., Roth, L., Seu, R., Shaffer, S., Soderblom, L., Stiles, B., Stofan, E., Vetrella, S., West, R., Wood, C., Wye, L., Zebker, H., 2005. Cassini Radar views the surface of Titan. Science 308, 970–974.

Elachi, C., Wall, S., Janssen, M., Stofan, E., Lopes, R., Kirk, R., Lorenz, R., Lunine, J., Paganelli, F., Soderblom, L., Wood, C., Wye, L., Zebker, H., Anderson, Y., Ostro, S., Allison, M., Boehmer, R., Callahan, P., Encrenaz, P., Flamini, E., Francescetti, G., Gim, Y., Hamilton, G., Hensley, S., Johnson, W., Kelleher, K., Muhleman, D., Picardi, G., Posa, F., Roth, L., Seu, R., Shaffer, S., Stiles, B., Vetrella, S., West, R., 2006. Titan Radar Mapper observations from Cassini's T3 fly-by. Nature 441, 709–713.

Fulchignoni, M., Ferri, F., Angrilli, F., Ball, A.J., Bar-Nun, A., Barucci, M.A., Bettanini, C., Bianchini, G., Borucki, W., Colombatti, G., Coradini, M., Coustenis, A., Debei, S., Falkner, P., Fanti, G., Flamini, E., Gaborit, V., Grard, R., Hamelin, M., Harri, A.M., Hathi, B., Jernej, I., Leese, M.R., Lehto, A., Lion Stoppato, P.F., Lpez-Moreno, J.J., Mkinen, T., McDonnell, J.A.M., McKay, C.P., Molina-Cuberos, G., Neubauer, F.M., Pirronello, V., Rodrigo, R., Saggin, B., Schwingenschuh, K., Seiff, A., Simes, F., Svedhem, H., Tokano, T., Towner, M.C., Trautner, R., Withers, P., Zarnecki, J.C., 2005. In situ measurements of the physical characteristics of Titan's environment. Nature 438, 785–791.

Graves, S.D.B., McKay, C.P., Griffith, C.A., Ferri, F., Fulchignoni, M., 2008. Rain and hail can reach the surface of Titan. Planetary and Space Science 56, 346–357.

Griffith, C.A., Hall, J.L., Geballe, T.R., 2000. Detection of daily clouds on Titan. Science 290, 509–513.

Griffith, C.A., Penteado, P., Baines, K., Drossart, P., Barnes, J., Bellucci, G., Bibring, J., Brown, R., Buratti, B., Capaccioni, F., Cerroni, P., Clark, R., Combes, M., Coradini, A., Cruikshank, D., Formisano, V., Jaumann, R., Langevin, Y., Matson, D., McCord, T., Mennella, V., Nelson, R., Nicholson, P., Sicardy, B., Sotin, C., Soderblom, L.A., Kursinski, R., 2005. The evolution of Titan's mid-latitude clouds. Science 310, 474–477.

Hayes, A., Aharonson, O., Callahan, P., Elachi, C., Gim, Y., Kirk, R., Lewis, K., Lopes, R., Lorenz, R., Lunine, J., Mitchell, K., Mitri, G., Stofan, E., Wall, S., 2008. Hydrocarbon lakes on Titan: distribution and interaction with a porous regolith. Geophysical Research Letters 35, L09204.

Hayes, A., Wolf, A., Aharonson, O., Zebker, H., Lorenz, R., Kirk, R., Paillou, P., Lunine, J., Wye, L., Callahan, P., Wall, S., Elachi, C., 2010. Bathymetry and absorptivity of Titan's Ontario Lacus. Journal of Geophysical Research 115, E09009.

Hueso, R., Sanchez-Lavega, A., 2006. Methane storms on Saturn's moon Titan. Nature 442, 428–431.

Jaumann, R., Brown, R.H., Stephan, K., Barnes, J.W., Soderblom, L.A., Sotin, C., Le Mouelic, S., Clark, R.N., Soderblom, J., Buratti, B.J., Wagner, R., McCord, T.B., Rodriguez, S., Baines, K.H., Cruikshank, D.P., Nicholson, P.D., Griffith, C.A.,

Langhans, E., Lorenz, R.D., 2008. Fluvial erosion and post-erosional processes on Titan. Icarus 197, 526–538.
Janssen, M.A., Lorenz, R.D., West, R., Paganelli, F., Lopes, R.M., Kirk, R.L., Elachi, C., Wall, S.D., Johnson, W.T.K., Anderson, Y., Boehmer, R.A., Callahan, P., Gim, Y., Hamilton, G.A., Kelleher, K.D., Roth, L., Stiles, B., Le Gall, A., 2009. the Cassini Radar Team, 2009. Titan's surface at 2.2-cm wavelength imaged by the Cassini Radar radiometer: calibration and first results. Icarus 200, 222–239.
Jennings, D.E., Flasar, F.M., Kunde, V.G., Samuelson, R.E., Pearl, J.C., Nixon, C.A., Carlson, R.C., Mamoutkine, A.A., Brasunas, J.C., Guandique, E., Achterberg, R.K., Bjoraker, G.L., Romani, P.N., Segura, M.E., Albright, S.A., Elliott, M.H., Tingley, J.S., Calcutt, S., Coustenis, A., Courtin, R., 2009. Titan's surface brightness temperatures. Astrophysical Journal 691, L103–L105.
Kouvaris, L.C., Flasar, F.M., 1991. Phase equilibrium of methane and nitrogen at low temperatures: application to Titan. Icarus 91, 112–124.
Lopes, R.M.C., Mitchell, K.L., Stofan, E.R., Lunine, J.I., Lorenz, R., Paganelli, F., Kirk, R.L., Wood, C.A., Wall, S.D., Robshaw, L.E., Fortes, A.D., Neish, C.D., Radebaugh, J., Reffet, E., Ostro, S.J., Elachi, C., Allison, M.D., Anderson, Y., Boehmer, R., Boubin, G., Callahan, P., Encrenaz, P., Flamini, E., Francescetti, G., Gim, Y., Hamilton, G., Hensley, S., Janssen, M.A., Johnson, W.T.K., Kelleher, K., Muhleman, D.O., Ori, G., Orosei, R., Picardi, G., Posa, F., Roth, L.E., Seu, R., Shaffer, S., Soderblom, L.A., Stiles, B., Vetrella, S., West, R.D., Wye, L., Zebker, H.A., 2007a. Cryovolcanic features on Titan's surface as revealed by the Cassini Titan Radar Mapper. Icarus 186, 395–412.
Lopes, R.M.C., Mitchell, K.L., Wall, S.D., Mitri, G., Janssen, M., Ostro, S.J., Kirk, R.L., Hayes, A., Stofan, E.R., Lunine, J.I., Lorenz, R., Wood, C.A., Radebaugh, J., Paillou, P., Zebker, H.A., Paganelli, F., 2007b. the Cassini RADAR Team, 2007. The lakes and seas of Titan. Transactions of EOS, American Geophysical Union 88, 569–576.
Lopes, R.M.C., Stofan, E.R., Peckyno, R., Radebaugh, J., Mitchell, K.L., Mitri, G., AWood, C.A., Kirk, R.L., Wall, S.D., Lunine, J.I., Hayes, A., Lorenz, R., Farr, T., Wye, L., Craig, J., Ollerenshaw, R.J., Janssen, M., Legall, A., Paganelli, F., West, R., Stiles, B., Callahan, P., Anderson, Y., Valora, P., Soderblom, L., 2010. the Cassini RADAR Team, 2010. Distribution and interplay of geologic processes on Titan from Cassini radar data. Icarus 205, 540–558.
Lorenz, R.D., 1993. The life, death and afterlife of a raindrop on Titan. Planetary and Space Science 41, 647–655.
Lorenz, R.D., Griffith, C.A., Lunine, J.I., McKay, C.P., Renn, N.O., 2005. Convective plumes and the scarcity of Titan's clouds. Geophysical Research Letters 32, L01201.
Lorenz, R.D., Lopes, R.M., Paganelli, F., Lunine, J.I., Kirk, R.L., Mitchell, K.L., Soderblom, L.A., Stofan, E.R., Ori, G., Myers, M., Miyamoto, H., Radebaugh, J., Stiles, B., Wall, S.D., Wood, C.A., Team, T.C.R., 2008. Fluvial channels on Titan : initial Cassini radar observations. Planetary and Space Science 56, 1132–1144.
Lunine, J.I., Stevenson, D.J., Yung, Y.L., 1983. Ethane ocean on Titan. Science 222, 1229–1230.
Mitri, G., Showman, A.P., Lunine, J.I., Lorenz, R.D., 2007. Hydrocarbon lakes on Titan. Icarus 186, 385–394.
Nelson, R.M., Kamp, L.W., Lopes, R.M.C., Matson, L., Kirk, R., Hapke, B., Wall, S.D., Boryta, M.D., Leader, F.L., Smythe, W.D., Mitchell, K., Baines, K.H., Jaumann, R., Sotin, C., Clark, R.N., Cruickshank, D.P., Drossart, P., Lunine, J., Combes, M., Bellucci, G., Bibring, J.-P., Capaccioni, F., Cerroni, P., Coradani, A., Formasiano, V., Filacchione, G., Langevin, Y., McCord, T., Menella, V., Nicholson, P.D., Sicardy, B., Itrwin, P.J., Pearl, J.C., 2009. Photometric changes on Saturn's Titan: evidence for active cryovolcanism. Geophysical Research Letters 36, L04202.
Notarnicola, C., Ventura, B., Casarano, D., Posa, F., 2009. Cassini radar data: estimation of Titan's lake features by means of Bayesian inversion algorithm. IEEE Transactions on Geoscience and Remote Sensing 47, 1503–1511.
Perron, J.T., Lamb, M.P., Koven, C.D., Fung, I.Y., Yager, E., Adamkovics, M., 2006. Valley formation and methane precipitation rates on Titan. Journal of Geophysical Research 111, E11001.
Radebaugh, J., Lorenz, D., Kirk, R.L., Lunine, J.I., Stofan, E.R., Lopes, R.M.C., Wall, S.D., 2007. the Cassini Radar Team, 2007. Mountains on Titan observed by Cassini Radar. Icarus 192, 77–91.
Radebaugh, J., Lorenz, R.D., Lunine, J.I., Wall, S.D., Boubin, G., Reffet, E., Kirk, R.L., Lopes, R.M., Stofan, E.R., Soderblom, L., Allison, M., Janssen, M., Paillou, P., Callahan, T., Spencer, C., The Cassini Radar, T., 2008. Dunes on Titan observed by Cassini Radar. Icarus 194, 690–703.
Raulin, F., 2008. Planetary science: organic lakes on Titan. Nature 454, 587–589.
Reh, K., Lunine, J., Matson, D., Magner, T., Lebreton, J.-P., Coustenis, A., 2008. TSSM Final Report on the NASA Contribution to a Joint Mission with ESA, JPL D-48148, NASA Task Order NMO710851.
Richards, J.A., 1999. Remote Sensing Digital Image Analysis. Springer-Verlag, Berlin, p. 240.
Soderblom, L.A., Tomasko, M.G., Archinal, B.A., Becker, T.L., Bushroe, M.W., Cook, D.A., Doose, L.R., Galuszka, D.M., Hare, T.M., Howington-Kraus, E., Karkoschka, E., Kirk, L., Lunine, J.I., McFarlane, E.A., Redding, B.L., Rizk, B., Rosiek, M.R., See, C., Smith, P.H., 2007. Topography and geomorphology of the Huygens landing site on Titan. Planetary and Space Science 55, 2015–2024.
Soderblom, L.A., Brown, R.H., Soderblom, J.M., Barnes, J.W., Kirk, R.L., Sotin, C., Jaumann, R., Mackinnon, d.J., Mackowski, D.W., Baines, K.H., Buratti, B.J., Clark, R.N., Nicholson, P.D., 2009. The geology of Hotei Regio, Titan: correlation of Cassini VIMS and RADAR. Icarus 204, 610–618.
Sotin, C., 2007. Planetary science: Titan's lost seas found. Nature 445, 29–30.
Stofan, E.R., Elachi, C., Lunine, J.I., Lorenz, R.D., Stiles, B., Mitchell, K.L., Ostro, S., Soderblom, L., Wood, C., Zebker, H., Wall, S., Janssen, M., Kirk, R., Lopes, R., Paganelli, F., Radebaugh, J., Wye, L., Anderson, Y., Allison, M., Boehmer, R., Callahan, P., Encrenaz, P., Flamini, E., Francescetti, G., Gim, Y., Hamilton, G., Hensley, S., Johnson, W.T.K., Kelleher, K., Muhleman, D., Paillou, P., Picardi, G., Posa, F., Roth, L., Seu, R., Shaffer, S., Vetrella, S., West, R., 2007. The lakes of Titan. Nature 445, 61–64.
Thompson, W.R., Zollweg, J.A., Gabis, D.H., 1992. Vapor–liquid equilibrium thermodynamics of N_2 + CH_4—model and Titan applications. Icarus 97, 187–199.
Tobie, G., Grasset, O., Lunine, J.I., Mocquet, A., Sotin, C., 2005. Titans internal structure inferred from a coupled thermal-orbital model. Icarus 175, 496–502.
Tokano, T., McKay, C.P., Neubauer, F.M., Atreya, S.K., Ferri, F., Fulchignoni, M., Niemann, H.B., 2006. Methane drizzle on Titan. Nature 442, 432–435.
Tomasko, M.G., Archinal, B., Becker, T., Bezard, B., Bushroe, M., Combes, M., Cook, D., Coustenis, A., de Bergh, C., Dafoe, L.E., Doose, L., Doute, S., Eibl, A., Engel, S., Gliem, F., Grieger, B., Holso, K., Howington-Kraus, E., Karkoschka, E., Keller, H.U., Kirk, R., Kramm, R., Kuppers, M., Lanagan, P., Lellouch, E., Lemmon, M., Lunine, J., McFarlane, E., Moores, J., Prout, G.M., Rizk, B., Rosiek, M., Rueffer, P., Schroder, S.E., Schmitt, B., See, C., Smith, P., Soderblom, L., Thomas, N., West, R., 2005. Rain, winds and haze during the Huygens probe's descent to Titan's surface. Nature 438, 765–778.
Toon, O.B., McKay, C.P., Courtin, R., Ackerman, T.P., 1988. Methane rain on Titan. Icarus 75, 255–284.
Turtle, E.P., Perry, J.E., McEwen, A.S., DelGenio, A.D., Barbara, J., West, R.A., Dawson, D.D., Porco, C.C., 2009. Cassini imaging of Titan's high-latitude lakes, clouds, and south-polar surface changes. Geophysical Research Letters 36, L02204.
Ulaby, F.T., Moore, R.K., Fung, A.K., 1982. Microwave Remote Sensing: Active and Passive, vol. 2. Artech House, Norwood, Mass.
Wall, S.D., Lopes, R.M.C., Stofan, E.R., Wood, C.A., Radebaugh, J.L., Horst, S.M., Stiles, B.W., Nelson, R.M., Kamp, L.W., Janssen, M.A., Lorenz, R.D., Lunine, J.I., Farr, T.G., Mitri, G., Paillou, P., Paganelli, F., Mitchell, K.L., 2009. Cassini RADAR images at Hotei Arcus and western Xanadu, Titan: evidence for geologically recent cryovolcanic activity. Geophysical Research Letters 36, L04203.
Wall, S., Hayes, A., Bristow, C., Lorenz, R., Stofan, E., Lunine, J., Le Gall, A., Janssen, M., Lopes, R., Wye, L., Soderblom, L., Paillou, P., Aharonson, O., Zebker, H., Farr, T., Mitri, G., Kirk, R., Mitchell, K., Notarnicola, C., Casarano, D., Ventura, B., 2010. Active shoreline of Ontario Lacus, Titan: a morphological study of the lake and its surroundings. Geophysical Research Letters 37, L05202.
Wood, C.A., Lorenz, R., Kirk, R., CLopes, R.M., Mitchell, K.L., Stofan, E., 2010. Impact craters on Titan. Icarus 206, 334–344.
Wye, L., Zebker, H.A., Hayes, A.G., Lorenz, R.D., Notarnicola, C., Ventura, B., Casarano, D., the Cassini Radar Team, 2010. Constraining depths and wave heights for Titan's lakes with Cassini RADAR Data. In: American Geophysical Union, Fall Meeting 2010, abstract P31C-1552.